IJE TRANSACTIONS B: Applications Vol. 35, No. 05, (May 2022) 883-899

International Journal of Engineering

Journal Homepage: www.ije.ir

Experimental Study on Performance Assessment of Hydraulic Power Take-off System in Centipede Wave Energy Converter Considering Caspian Sea Wave Characteristics

M. Aghanezhad, R. Shafaghat*, R. Alamian, S. M. A. Seyedi, M. J. Raji Asadabadi

Sea-Based Energy Research Group, Babol Noshirvani University of Technology, Babol, Iran

PAPER INFO

Paper history:
Received 13 January 2022
Received in revised form 29 January 2022
Accepted 01 February 2021

Keywords:
Centipede Wave Energy Converter
Hydraulic Power Take-off System
Experimental Study
Wave Tank
Simcenter Amesim

ABSTRACT

Considering the characteristics of the Caspian Sea waves, using a centipede wave energy converter might lead to satisfactory performance. The present paper introduced a pilot wave energy converter (WEC) called IRWEC2. Moreover, the performance of the hydraulic power take-off (PTO) system developed for the WEC was assessed experimentally in the wave tank of Babol Noshirvani University of Technology (BNUT). The Simcenter Amesim software was used so as to design the hydraulic PTO system and to initially evaluate the system performance. For two separate buoys were used, different series and parallel configurations were employed for the separate hydraulic cylinders connected to each buoy to achieve the optimum performance of the PTO system. The characteristics of input wave, resistant load, and flow control valve opening were defined as the most important parameters affecting the converter performance. Accordingly, the maximum value of generator output was obtained based on the certain values of these parameters. To validate the processes defined, the simulation results obtained through the Simcenter Amesim software were compared to the experimental ones and a good agreement was found. According to the results, the maximum power of the PTO system was 46 watts (for laboratory scale), which is related to the parallel configuration. In this case, the efficiency of the PTO system was 23%. Moreover, the output of the generator increased by about 12% compared to the case where only one buoy was used.

***doi**: 10.5829/ije.2022.35.05b.05*

NOMENCLATURE

a	Amplitude (cm)	$\bar{x}$	Average of measured data
A	Piston area (mm^2)	x_i	Measured data
F	Applied force to the cylinder (N)	**Greek Symbols**	
GDP	Generator dissipation (%)	v	Piston velocity ($^m/_s$)
I	electric current (A)	ΔP	Pressure difference (bar)
N	Experiment perform number	Δx	Piston displacement (cm)
P_G	Output generator power (W)	Δy	Buoy displacement (cm)
P_{HM}	Output hydromotor power (W)	ω	Angular frequency ($^{rad}/_s$)
P_{in}	Applied power to the cylinder (W)	ω_{out}	Rotational velocity (for G & HM) (RPM)
P	Hydraulic cylinder pressure (bar)	$\omega_{W.M}$	Wave maker angular frequency ($^{rad}/_s$)
Q	Hydromotor flowrate ($^l/_{min}$)	σ_m	Standard uncertainty
RPM	Wave maker rotational velocity (RPM)	η_{PTO}	PTO Efficiency (%)
s	Standard deviation	η_t	Hydromotor Efficiency (%)
t	Time (s)	**Subscripts**	
T	Period (s)	G	Generator
V	Voltage (V)	HM	HydroMotor
V_g	Displacement (cm^3)	i	Data item
		W.M	Wave Maker

*Corresponding Author Institutional Email: rshafaghat@nit.ac.ir (R. Shafaghat)

Please cite this article as: M. Aghanezhad, R. Shafaghat, R. Alamian, S. M. A. Seyedi, M. J. Raji Asadabadi, Experimental Study on Performance Assessment of Hydraulic Power Take-off System in Centipede Wave Energy Converter Considering Caspian Sea Wave Characteristics, ***International Journal of Engineering, Transactions B: Applications***, Vol. 35, No. 05, (2022) 883-899

1. INTRODUCTION

Nowadays, using renewable energy is among the programs and policies of developed and developing countries. With their significant energy density, the waves of seas and oceans are known as one of the sustainable subsets of renewable energy sources [1]. A variety of methods to harness the energy of seas' and oceans' waves have been submitted in the form of hundreds of ideas and research works. It is worth mentioning that many ideas and designs have been utilized as the final product as wave energy converters (WECs). Considering every single of the energy absorption mechanisms, WECs can have different power take-off (PTO) systems. Mechanical, pneumatic, hydraulic PTOs and also direct power transmision system are different types as following researchers studied. Tri et al. [2] used such a mechanical PTO system driven by a continuously variable transmision system (CVT) for point absorber type WEC. Yazdi et al. [3] studied pnumatic one in OWC WEC. Henderson [4] tested hydraulic PTO in Pelamis. Waters et al. [5] examined a linear generator configured with a buoy and sea cable. Centipede wave energy converters are designed to use an array of buoys to attain wave energy. Each of these absorbent units is attached to an arm as the first element of the PTO chain to transmit the heave motion, which is created in the primary interaction (PI) with the wave, to the other components of the PTO system (see Figure 1). At the end of the PTO chain, the reciprocating motions of the buoy are converted into rotational motion and accordingly electrical energy in a generator. The PTO system in a centipede converter could be mechanical, hydraulic, or direct (linear generators). The mechanical PTO system tends to be used in laboratory studies. In the semi-industrial and industrial models, hydraulic PTO systems are commonly utilized. The operational nature of the hydraulic PTO systems is appropriately in accordance with the attributes of sea waves. Using the hydraulic PTO systems in wave energy converters is very prevalent, amongst which Wavestar, Pelamis, AW-Energy, SEAREV, and ETC can be mentioned [6]. In this study, a hydraulic PTO system was utilized for the centipede WEC.

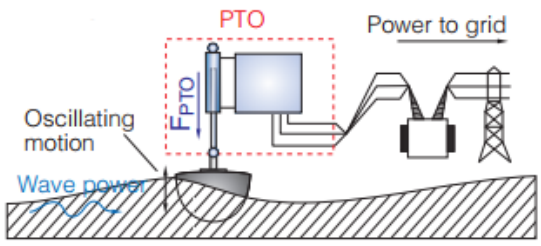

Figure 1. Primary interaction between absorber and wave to produce useful power electricity (wave to wire scheme) [7]

A great deal of research has been conducted on WECs, a part of which has been relevant to the absorber's shape, type, and connection method, and the other part deals with the optimization and control of the PTO system.

Sarlak et al. [8] numerically assessed the hydrodynamic parameters, efficiency, and dynamic response for different geometric shapes. Their results demonstrated that the horizontal cylinder shape is the most optimal geometry for the Offshore Wave Buoy WEC system between all samples. Alamian et al. [9] conducted a similar study utilizing NEMOH software for a point absorber converter. In this study, the optimization of the geometric shape considering its construction costs was investigated.

Babarit et al. [10] studied the two-way cylinder in a PTO system and used a gas accumulator to prevent fluctuations. Hansen et al. [11] also examined two different combinations in cylinders to control the power absorption by single and multiple point absorbers. One of the two systems studied was a symmetrical cylinder system with two oil chambers, and the other system contained two cylinders and four nonsymmetrical oil chambers that were tested in three different sea conditions. Cargo et al. [12] evaluated a type of point absorber WEC through numerical simulation in both ideal conditions and conditions with the loss. They achieved the optimal state by changing the features of some components of the hydraulic circuit. Moreover, their results indicated that there is no difference between optimization in the ideal circuit and the circuit with loss. This can assist in the numerical research to optimize the circuit of hydraulic transmission systems. Bayani et al. [13] used a wide variety of wave characteristics to examine the IRWEC1 in BNUT's wave tank. Considering the 1:8 scale, 145 kilowatts power is expected. Hassan et al. [14] used different configuration of turbines during a virtual experiment. In an experimental study, Coiro et al. [15] examined two different configurations of point absorbers in the two positions of the buoyant arm, one in the parallel position to the water surface and the other being angled to the water surface. Alamian et al. [16] utilized various mechanical PTO systems for the centipede wave converter system such as axles and flywheels, gear systems, and also wheels and chains, to name but a few. Another sample of a mechanical combination was conducted by Tri et al. [2]. They tested a system, including a CVT (continuously variable transmission) gearbox, a flywheel, and a WEC-CVT-EHA electrohydraulic actuator. Using an electrohydraulic system to maintain the generator at the rated speed, they dramatically increased the converter efficiency. In both configurations, the hydraulic cylinder is perpendicular to the arm. They also re-conducted this research numerically with two methods of potential theory and

URANS to parametrically analyze the system. Liu et al. [17] carried out an experimental and numerical examination of the hydraulic PTO system of the Pelamis wave energy converter in Aqua software and delineated the effect of different hydraulic parameters. They investigated the effect of several parameters, including the rod-to-piston diameter ratio, various wave conditions at sea, hydromotor displacement volume, and accumulator volume, on the efficiency. Kim et al. [18] tested a WEC, consisting of two hemispherical buoys with the same geometric attributes to maximize the power, that can be extracted in different positions in terms of the distance between the buoys and the pressure difference in the hydraulic motor. Other parameters investigated on the aforementioned wave converter system were the collision wave angle with the wave converter under different wave frequencies. Tian et al. [19] first modeled the small-scale impact (WEC) system by Simulink in MATLAB and then validated it. They used a combined electrohydraulic system to transmit power. Another parameter they studied was the pre-charged accumulator gas pressure. Aghanezhad et al. [20] defined dry tests to study the hydraulic PTO system of a centipede wave converter and examined various parameters to optimize the output power.

To utilize any PTO system in a WEC, it is of utmost importance to pay attention to crucial factors such as sea wave attributes, environmental conditions, and the compatibility of power transmission chain elements. This topic, coupled with the lack of sufficient maturity during using the industrial samples of wave energy converters [6], reveals the need to study and search on tuning and optimizing the PTO system more than ever. In some cases, replacing equipment, adjusting processes, or changing the configuration of PTO systems can improve the performance. In a centipede WEC, these changes can include changes in the size and shape of the absorber buoy, the length of the buoy arm, the size and volume of the hydraulic motor and accumulator, the settings of some parameters (e.g., accumulator pre-charge pressure, flow control valve opening), and resistive load determined for generator and hydraulic motor.

In order to optimize the hydraulic PTO system, it should be inspected in various conditions, and its dependence on effective parameters should also be considered. In this research, the centipede WEC having a hydraulic PTO system was assessed experimentally and numerically. To this end, the operation of the PTO system in the different conditions of the wave, resistive load, and the characteristics of hydraulic elements of the hydraulic circuit will be regarded. In light of the nature of centipede converters, two buoys were utilized together with two separate PTO systems. Thus, to evaluate the performance of the converter, different configurations of the two converters together with the two PTO systems were used. It is noteworthy that two hydraulic cylinders in different series and parallel positions were inspected to acquire an effectual output in different configurations. By choosing the best configuration using the Simcenter Amesim program, the output power of the PTO system was calculated while the appropriate number of buoys and cylinders were configured. Experimental data were used to validate the simulation results. It should be noted that the output power of the converter significantly depended on the features of the input wave. Accordingly, all changes in the system were made considering constant input waves so that the results were comparable.

2. MATERIALS AND METHODS

2. 1. Problem Statement In this research, the hydraulic PTO system in the IRWEC2 centipede WEC was assessed experimentally and numerically. To conduct experimental tests, considering the waves of the Caspian Sea, the wave tank of Babol Noshirvani University of Technology (BNUT) was utilized [21]. However, the laboratory study phase of this converter equipped with a mechanical PTO system was completed for two different arrays, including 6 and 10 buoys (see Figure 2). In order to complete laboratory tests and to approach the industrial model, the hydraulic PTO system was used due to the favorable features and performance of the hydraulic PTO system and its appropriate adaptation to the attributes of sea waves (see Figure 3). At this step, to ensure the performance of the hydraulic PTO system, the performance of the system in dry tests outside the tank was examined [20].

As mentioned before, a converter with two hemispherical buoys was used. The diameter of the both buoys was 110 cm, which was connected to the rotary joint using a 2.5m arm. The hydraulic cylinder connection point to the arm was considered at a point between the buoy and the rotary joint. To install the converter in the wave tank, it was essential to adjust the movement of the hydraulic cylinder. The hydraulic cylinder's movement stroke depends on the depth of water and the characteristics of the incoming waves. Figure 4 shows one of the converters installed in the tank. To accomplish the converter's appropriate performance points, two objective functions of the WEC efficiency and the output power were assessed. Various strategies were used in the experimental study to enhance the performance of the converter.

2. 2. Caspian Sea As mentioned earlier, to assess the performance of the centipede WEC, the characteristics of the Caspian Sea waves were considered. The Caspian Sea has significant potential to generate electricity from waves. Figure 5 demonstrates a combined diagram of wave distribution and energy according to two parameters of significant wave height and wave period in

the Caspian Sea in the beach of Babolsar city. The colored scale embodies the total annual energy per wavefront length unit, and the bold numbers indicate the probability of occurrence of any particular wave conditions according to the number of hours per year. As shown in Figure 5, the waves with a significant height of 0.5 to 1 m and a period of 4 to 6 seconds have the highest annual energy. However, another significant category of waves is the waves with a height of 0 to 0.5 meters and a period of 2 to 4 seconds, which are most likely to occur in the Caspian Sea (see Table 1).

Figure 2. Centipede WEC constructed and tested in BNUT, at Sea-based Energy Research group test rig by mechanical PTO system in 6 and 10 buoy arrays [20]

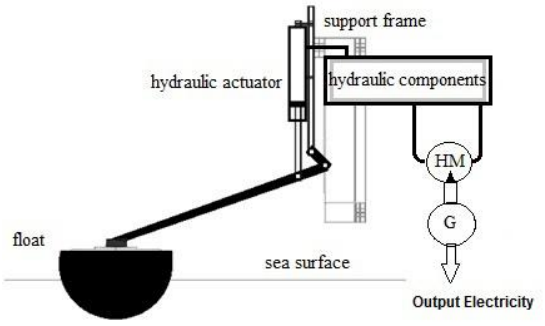

Figure 3. Centipede WEC scheme whit hemisphere buoy and hydraulic PTO system [20]

Figure 4. installation mode of centipede WEC in the wave tank

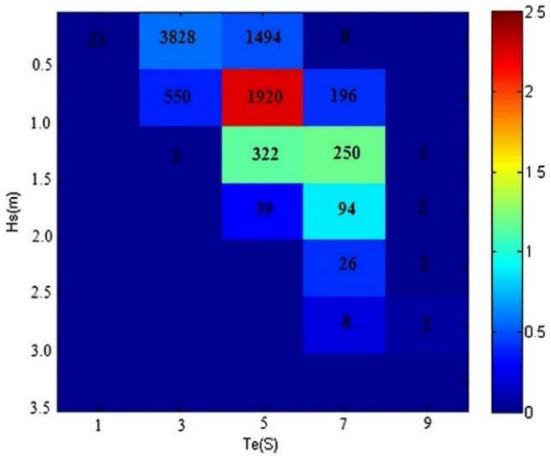

Figure 5. Combined scatter and energy diagrams of the annual energy corresponding to sea states in different ranges of Hs and Te for Caspian Sea (near Babolsar) [16]

TABLE 1. Caspian Sea wave classification for tests

Waves	Period (s)	Height (m)
Class I	4-6	0.5-1
Class II	2-4	0-0.5

To model the waves in the wave tank, it is very important to consider the WEC scaling. In this study, for the developed semi-industrial sample was used directly in the sea, the scale of the converter was 1:1, and the dimensions of the buoys in the experimental tests were equal to those of the buoys installed in the sea. Therefore, the wave characteristics will not be different compared to the sea wave features. Furthermore, the second group of waves prsented in Table 1 was used for experimental tests (class II). To this end, to implement the final tests in most of the experiments, a wave with a height of 40 cm and a period of 3 seconds was utilized in the wave tank.

Nevertheless, the stronger and weaker waves were also used whenever they were required.

2. 3. Experimental Study

2. 3.1. Experimental Equipment According to the energy transmission chain initiated from the sea waves, the centipede WEC was composed of various subsets and components (see Table 2). The mechanical components of the converter were a buoy and an intermediary arm to transmit the motion. In this converter, after the collision of the input wave, the wave energy was absorbed by the buoy and was then transferred by the arms to the hydraulic cylinder. The increased pressure of working fluid in the hydraulic cylinders was transferred to a hydromotor, which allowed the reciprocating motion of waves to convert into rotational motion. A single-acting hydraulic cylinder was applied in the system, generating the power only when the buoy moved upward followed by the arm. At the end of the process, mechanical energy was converted into electrical one by transferring the rotational motion to the generator. A schematic of the electrical circuit is shown in Figure 6.

Based on the energy conversion chain, the proper selection of elements for hydraulic PTO system and correct adjustment of them are of great importance. Figure 7 shows a schematic of the hydraulic power transmission system. As can be seen, check valves are considered on both sides of the hydraulic cylinder to prevent backflow generation. Moreover, an accumulator was used to reduce the fluctuations.

TABLE 2. The technical information of setup components

Item	Properties	
Buoy	Diameter	110 cm
	Draft	45.7 cm
	Weight	63 kg
Arm	Length	2.5 m
	Weight	16.3 kg
Hydraulic Cylinder	Piston Diameter	18 mm
	Cylinder Diameter	40 mm
	Stroke	245 mm
Oil Tank	Capacity	50 lit
Check valve	¾ and ¼ inch	
Accumulator	Nominal Capacity	2.5 lit
Relief valve	Pressure relief valve set at 15 bar	
Throttle valve	Needle valve	
Hydromotor	Type	Gerotor-fixed displacement
	Displacement	12.5 cc
Generator	Synchronous permanent magnet (AFPMG) (100W, 100RPM)	
Hydraulic oil	HLP 51524 part 2	
Rheostat	50 Ω, 50 V, 5 A	
Resistors	10 Ω, 10 W	

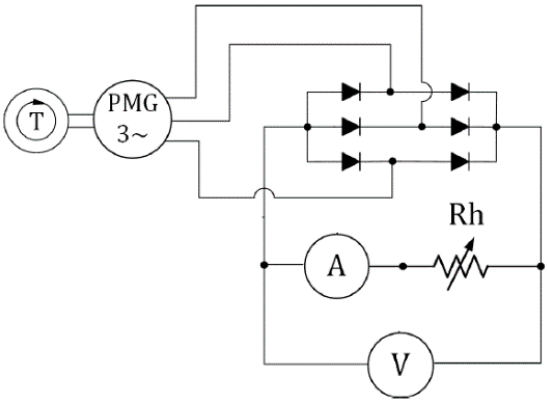

Figure 6. Electric circuit including Diode Bridge (bridge rectifier), rheostat and voltage and current measurement elements [20]

The technical specifications of measurement equipment with their accuracy range are presented in Table 3. Regarding the importance of knowing the wave characteristics and measuring the buoy fluctuations, analytical equations were used to determine the incident wave characteristics, and image analysis was employed to measure the buoyancy fluctuations. Tracker software was also used for image analysis. It should be mentioned that there was a red mark on the buoy for such a purpose, which was traceable to the software after capturing images and in the post-processing step. The incoming wave collision with the buoy and the piston movement made it possible to transfer the wave energy. An ultrasonic level-meter sensor was applied to measure the velocity and displacement of the piston. The force arising

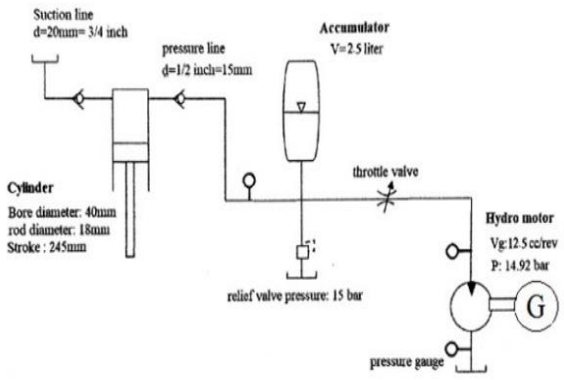

Figure 7. Schematic of hydraulic circuit and components [20]

TABLE 3. The technical information of measurement equipment

Item	Specification	Accuracy
Pressure Gauge	Dial type (10, 25, and 40 (bar))	±0.5%
Multimeter (voltage)	HIOKI 3256	±0.6%
Multimeter (current)	HIOKI 3200	±1.5%
Force Gauge	Radex digital weighing (50 kg)	±0.05%
Tachometer	Lutron tachometer DT-2268	±0.05%
Level meter	HC-SR04	±0.3 cm

from the wave in the hydraulic cylinder led to increasing the oil pressure in the hydraulic circuit. Several pressure gauges were employed to measure the oil pressure at different points of the hydraulic circuit. The output load was simulated using a rheostat and several resistors. Both voltage and current were measured by two multi-meters. Finally, the rotational speed of the generator and hydro-motor shafts was measured using a digital tachometer as shown in Figure 8.

An incident wave was produced in the form of regular waves by a paddle wave-maker system in a tank of dimensions 11 x 3 x 3 m (see Figure 9).

2. 3. 2. Uncertainty Analysis Because of numerous parameters measured and diversity of experiments, uncertainties were calculated for all measured data. The equations of average value, standard deviation, and mean dispersion were used to compute the percentage error of each quantity.

$$\bar{x} = \frac{\sum_{i=1}^{N} x_i}{N}$$
$$s = \sqrt{\frac{\sum_{i=1}^{N} (x_i - \bar{x})^2}{N-1}} \quad (1)$$
$$\sigma_m = \frac{s}{\sqrt{N}}$$

Figure 8. hydraulic and electric output data measurement equipment

Figure 9. overall view of wave tank [16]

where x_i is the measured data, $\bar{x}$ is the average of the measured data, N is the number of the performed experiments, and s and σ_m are the standard deviation and standard uncertainty parameters, respectively. As the experiments were repeated three times in each case, the uncertainty calculated for the voltage, flow, pressure, and rotational speed parameters are presented in Table 4.

Figure 10. Flow control valve and related settings for opening positions [20]

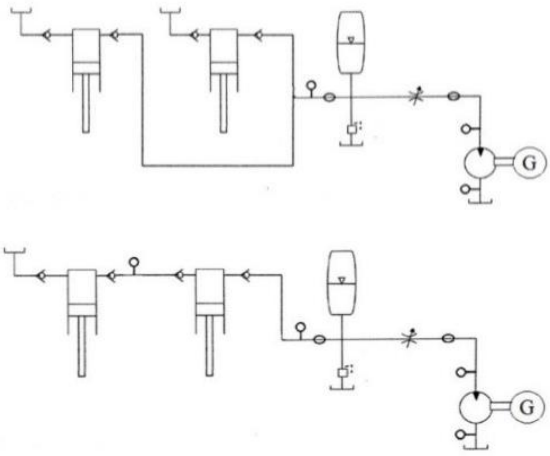

Figure 11. installation modes of parallel (a) and series (b) configurations

2. 3. 3. Test Method As mentioned above, a centipede WEC with two buoys was used where the tests were conducted for single-buoy and double-buoy cases. First, the tests were carried out for a single-buoy system. In this case, the effect of two parameters on the opening angle of the flow control valve and the output load was evaluated considering an incident wave with a height of 40 cm and a period of 3s. In these conditions, the goal was to achieve the maximum output power of the converter. As shown in Figure 10, the control valve opening angle was calibrated with the number of turns to open it. To this end, the odd number of turns was considered to adjust the opening angle of the flow control valve. The resistance variation was used in order to change the output load. In this regard, to determine the maximum throughput of the PTO system, the resistance changes starting from 20 ohms were increased by 10 ohms at each step. Thus, by determining proper operating points for the flow control valve and resistive load, it can be tested for other waves of heights 20, 25, and 30 cm.

Considering a buoy followed by a PTO system (a hydraulic cylinder), the wave height was determined by the most appropriate output and the optimum opening angle of the flow control valve. In the next step, the hydraulic cylinders of two separate PTO systems were tested in the series and parallel arrangements for double-buoy configuration.

The experimental steps are shown in Figure 12.

2. 3. 4. Output Data Processing To evaluate the performance of the IRWEC2 WEC, the converter output power was measured compared to the input power. The output power of the converter was determined by the measurement equipment; however, it was necessary to recognize the input wave characteristics to examine the input power to the WEC. Several desired waves were generated in the wave tank using a paddle wave-maker in which two inputs, including stroke length and wave-maker frequency, were applied to adjust it. The wave period was directly dependent on the wave-maker frequency on the basis of Equation (2); also, the wave height was adjusted by changing the stroke length.

$$RPM = \omega_{W.M} \times \frac{60}{2\pi} = \frac{2\pi}{T} \times \frac{60}{2\pi} = \frac{60}{T} \quad (2)$$

Table 5 shows the wave period for every single desired frequency of the wave-maker. Since the wave period for all experiments was assumed to be a fixed value of 3s, the waves with various heights could be generated by varying the wave-maker stroke (see Table 6). Each specific wave height was named according to its obtained value.

As the Wave Mode I experiment had the maximum wave height, it was considered to evaluate the conformance between the buoy fluctuations and the incoming wave conditions. To define the incoming wave based on the specified wave-maker frequency, the target wave height would be determined by varying the length of the wave-maker stroke. Therefore, Equation (3) could be applied to the incoming wave in this test; image

TABLE 4. uncertainty for all parameters in specific test condition (Wave Mode I, R=20 ohms, single configuration)

$N = 3$	V	I	$P_{cylinder}$	ΔP	ω_{out}
Certainty in 95% level	±2.82%	±0.03%	±0.76%	±0.60%	±7.25%

TABLE 5. wave period converted to RPM as an input

T (s)	1.5	2	2.15	2.4	2.6	3	3.5	4
RPM	40	30	28	25	23	20	17	15

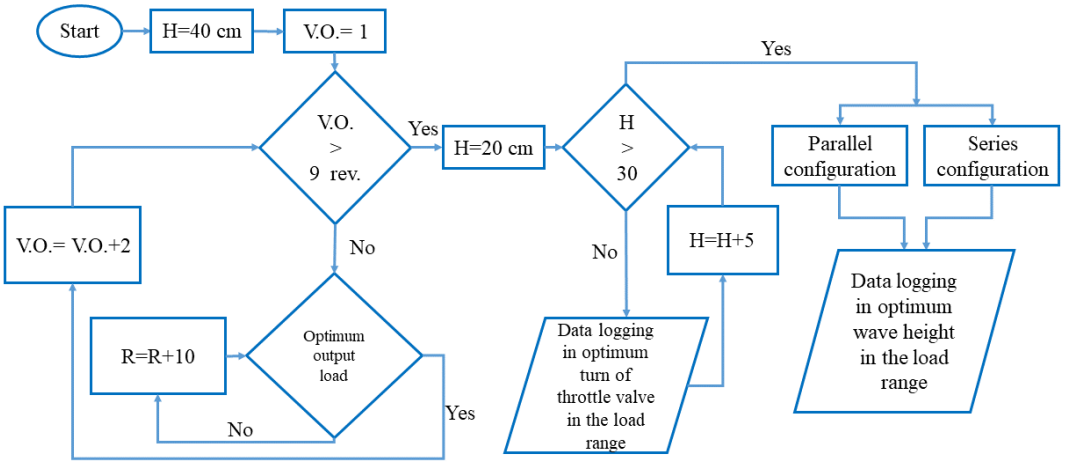

Figure 12. test flowchart

analysis was also used to evaluate the buoy fluctuations. Figure 13 depicts the comparison of the incoming wave profile and the buoy fluctuations.

$$y = \text{asin}(\omega t) = 20\sin(2.093t) \quad (3)$$

As discussed above, the buoy displacements directly affect the hydraulic cylinder performance. If the power transmitted from the buoy to the hydraulic cylinder is considered equivalent to the PTO input power, Equation (4) can be applied to calculate the input power.

$$P_{in} = F * v \quad (4)$$

where F is the piston force (N) obtained using the cylinder pressure (Equation 5), v is the piston average velocity (m/s), and P_{in} is the system input power (W).

$$F = \frac{P \times A}{10} \quad (5)$$

P is the cylinder pressure (bar) measured through the experiment, and A is the piston cross-sectional area (mm^2).

To obtain the piston average velocity, its displacement was first calculated using the level-meter sensor (see Figure 14), then the average velocity was calculated by given piston displacement in the hydraulic circuit charging stage and the piston displacement duration.

TABLE 2. nominated wave modes for tests

T (s)	H (cm)	Wave Mode (W.M.)
3	40	I
3	30	II
3	25	III
3	20	IV

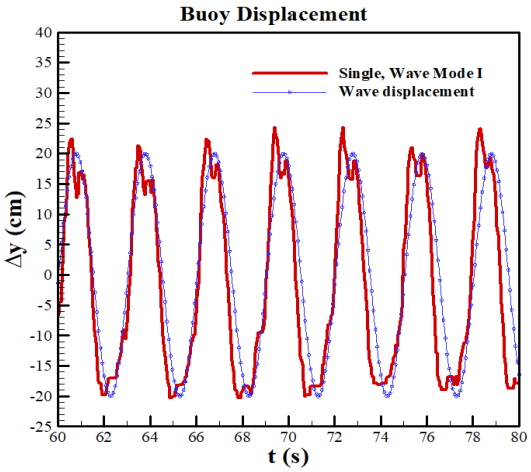

Figure 13. Buoy displacement due to wave motion W.M. I

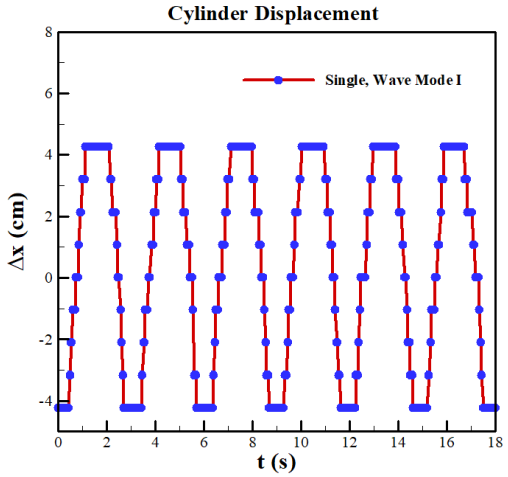

Figure 14. Piston displacement in W.M. I condition

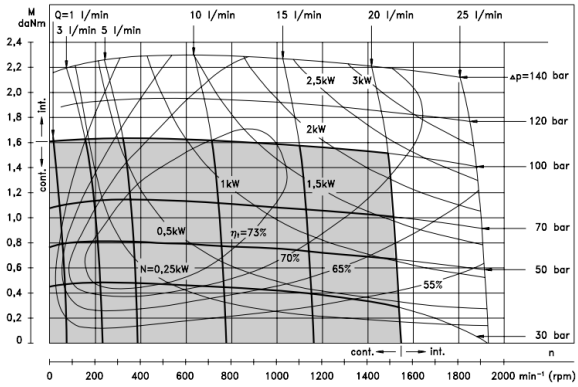

Figure 15. Hydromotor performance diagram [22]

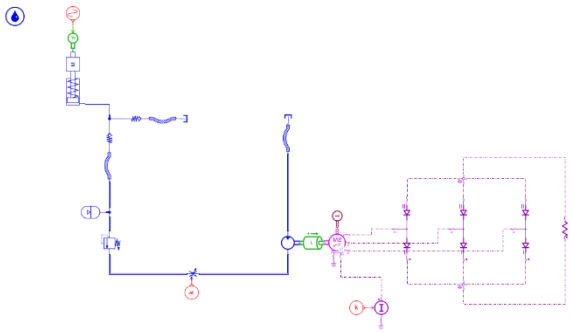

Figure 16. Amesim simulation diagram for hydraulic and electric circuits

After charging the hydraulic circuit by the buoy motion and the piston displacement in the hydraulic cylinder, a high-pressure fluid was transferred through the hydraulic circuit to the hydromotor. According to the information from the hydromotor manufacturer, the hydromotor power was obtained from Equation (6) [23]:

$$P_{HM}(w) = Q * \Delta p * \frac{\eta_t}{600} * 1000 \quad (6)$$

where Q denotes the volume flow rate passed through hydromotor ($^{l}/_{min}$), and Δp is the pressure difference between the hydromotor inlet and outlet (bar). The parameter η_t represents the efficiency of the hydromotor in different operating conditions that were calculated at all the operating points based on Figure 15 [22]. The flow rate passing through hydromotor was obtained from Equation (7):

$$Q\left(^{l}/_{min}\right) = \frac{\omega_{out}(RPM) * V_g(cm^3)}{1000} \quad (7)$$

where ω is the rotational speed of hydromotor measured in all different conditions through the experiments and V_g is a constant parameter indicating the displacement of hydromotor and is equal to 12.9 cm^3.

The hydromotor drived a generator to produce electric power. The output power of the generator, as the output power of the wave energy converter, was calculated by Equation (8):

$$P_G = I * V \quad (8)$$

where I is the electric current (A) and V is the voltage between the consumer ends (V).

The power transmission setting included some subsets such as plumbing, hydraulic cylinder, accumulator, throttle valve, relief valve, hydromotor, and generator, which every one of them could contribute to the power loss. Equation (9) was applied to obtain the overall efficiency of the PTO system:

$$\eta_{PTO} = \frac{P_G}{P_{in}} * 100 \quad (9)$$

where P_G is the output power of the generator and P_{in} is the input power to the hydraulic cylinder.

In addition to the overall efficiency of the PTO system, there is a parameter called generator power dissipation, which is the amount of power that is not converted to the useful power by the generator and coupling. The GDP parameter was employed to analyze this problem [20]:

$$GDP = \left(1 - \frac{P_G}{P_{HM}}\right) * 100 \quad (10)$$

2. 4. Numerical Study Simcenter Amesim software was utilized to initially design the hydraulic circuit and evaluate the performance of the hydraulic PTO system at the optimal operating points. In this regard, to evaluate the performance, different configurations were examined, including one hydraulic cylinder and two hydraulic cylinders, in series and parallel mode configurations. This software is a multi-purpose toolbox so as to model and analyze a system with various mechanical, electrical, and control components. Figure 16 shows, for example, the hydraulic and electric circuits of the PTO system simulated in Simcenter Amesim software.

In order to simulate the wave-induced force, a force transducer and an input signal were used to apply the wave sinusoidal motion. The incoming signal was set based on the force exerted on the buoy and its movement period. By defining this force, it was exerted to the cylinder through the force transducer. In this circuit, a single-acting cylinder was used according to the experimental prototype, and a cylinder-attached mass was considered in simulations due to the buoy and arm weights. All features of the hydraulic cylinder, including its internal dimensions, motion stroke, cylinder movement speed, and hydraulic fluid properties, were determined established upon the experimental prototype. The hydraulic circuit was considered similar to the experimental one. Furthermore, the hydromotor power was transmitted using a coupling to a generator. Concerning the defined electric circuit, it is possible to measure voltage and current as electrical outputs of the circuit.

2. 4. 1. Numerical Method Validation The results obtained from the Wave Mode I experiment were used to examine the validity of the simulation results. In the first step, to validate the numerical method, the single-buoy experimental tests were applied only. According to the circuit designed for this case, the outputs of the software, including the hydromotor pressure, voltage, and current and the generator power, are presented in Figure 17. It is worthy to mention that the outputs were extracted when the results were stabilized. The numerical and experimental results are in good agreement, so the numerical data errors were computed as 5.4, 5.7, and 6.5% for the differential pressure, voltage, and current of hydromotor, respectively. The electric power parameter was obtained by multiplying the voltage and current parameters.

According to the validation of the results obtained from the single-buoy case, validations are presented for several series and parallel configurations (see Figure 18). As can be seen, the experimental and simulation results are in good agreement; the mean difference between the experimental and simulation data is 5.4 and 6.4% in series and parallel modes, respectively.

3. RESULTS

In this section, the results of the experimental tests are presented. To this end, the WEC performance with a buoy is compared to the WEC with two buoys. It is worthy to note that about the WEC with two buoys, the results are presented for two parallel and series configurations. After selecting the more preferred

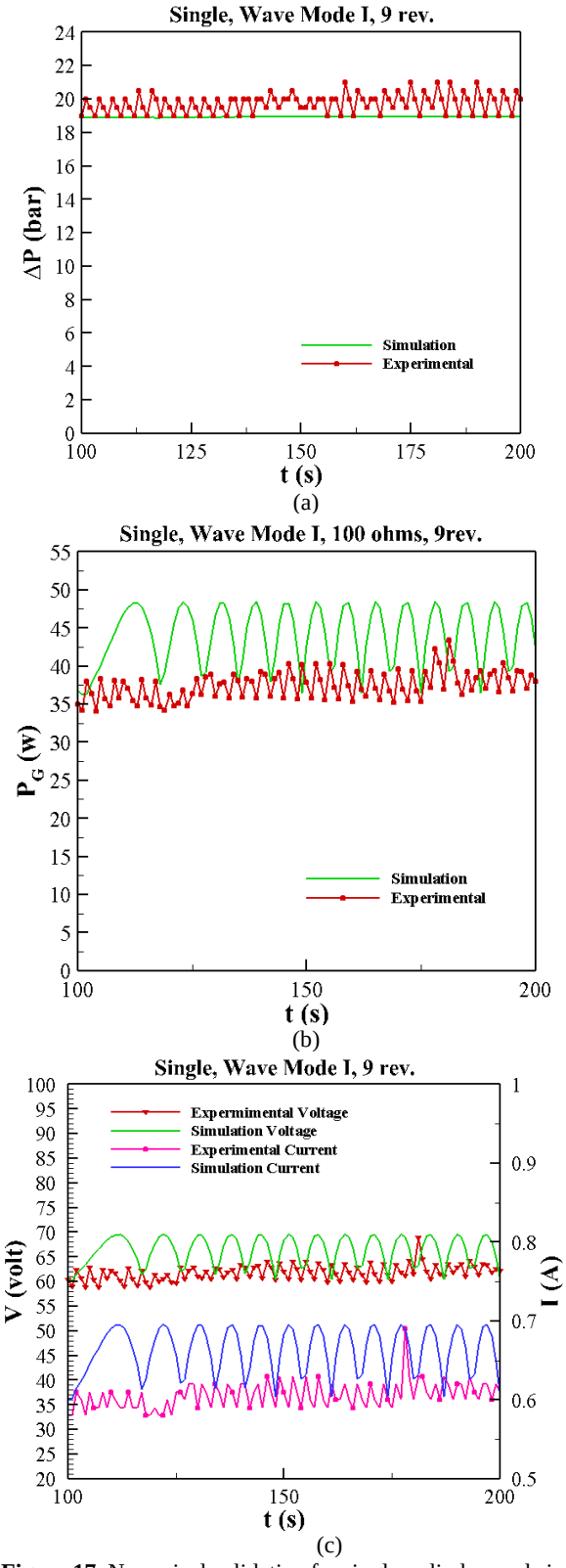

Figure 17. Numerical validation for single-cylinder mode in a 100-ohm resistance and 9 turns mode, a: experimental and numerical pressure results comparison, b: experimental and numerical power results comparison, c: experimental and numerical V and I results comparison

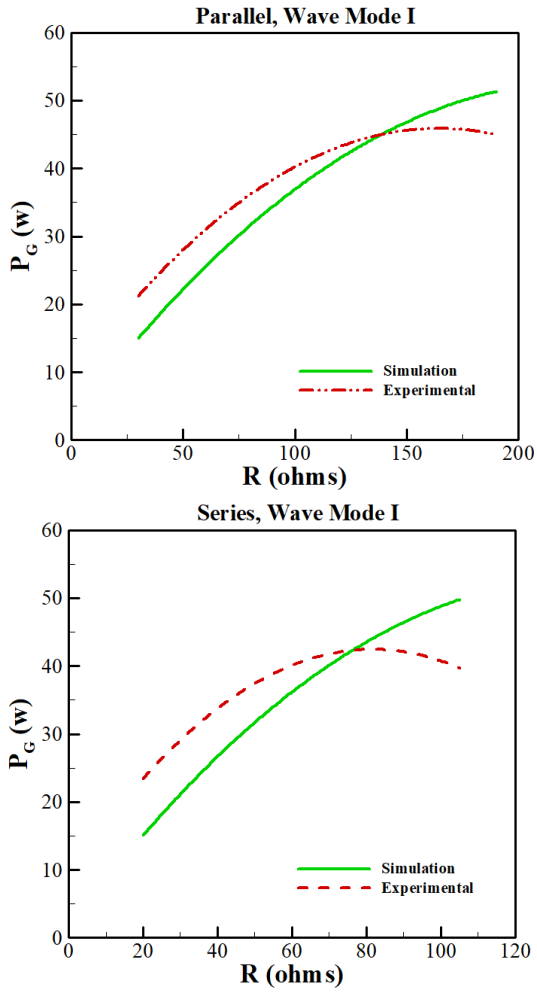

Figure 18. Parallel and series configuration validation

configuration in terms of performance, the results concerning Simcenter Amesim software are first validated with the experimental results, and the effect of an increased number of buoys is then examined for the selected configuration.

3. 1. Experimental Results To provide the experimental results, the results of the Wave Mode I experiment are first presented. In this experiment, the wave height and period were considered to be 40 cm and 3 seconds, respectively. Figure 19a shows the output power versus the resistive load of the rheostat for different opening modes of the flow control valve. According to Figure 19a, by increasing the rheostat resistance, the output power increases first to reach a maximum value, and the output power is fixed initially by a further increase in the resistance, and is then decreased gradually. The ideal output power is achieved as 41.37 W for a 100-ohm resistor and 9 turns of the flow control valve. It should be noted that the power increase in the resistance range from 20 to 100 ohms is equal to

153%, followed by a decreasing trend. Moreover, for a 100-ohm resistor, the output power for 9 turns of flow control valve increases by about 7.8% relative to 1 turn. Figure 19b shows that the experimental results are in good consistency with the simulation ones in such a way that the minimum difference is about 0.7% for an 80-ohm resistor and the maximum difference is about 18.8% for a 40-ohm resistor.

The hydromotor power is calculated using the flow rate passed through it. Figure 20 indicates the hydromotor output power in terms of the resistive load for different turns of the flow control valve. Similar to the generator power, the hydromotor maximum power is also achieved for a 100-ohm resistor, which is equivalent to 41.87 W. A negligible difference between the output power of hydromotor and generator indicates very low power losses.

Figure 21a shows the efficiency of the PTO system. The maximum efficiency of the PTO is calculated as 26% for a 100-ohm resistor and 9 turns of the flow control valve. This value is as approximately the same as a 105-ohm resistor. The efficiency curve unlike the power curves has an ascending trend. It seems that by increasing the resistive load, efficiency increases, but it is not considerable due to the loss of the generator output power and the interruption of the output power. Figure 21b shows the loss curves between the hydromotor and the generators for various opening modes. Based on the presented plots, it is observed that the curves' trend is the same for the rest of the cases except for one turn of the flow control valve.

The reason of this difference is attributed to the significant losses of the system to open the flow control valve in one turn. It should be mentioned that in the maximum values of the output power and efficiency, the power loss is negligible, almost equal to zero. This power loss is an indication of the power that the generator

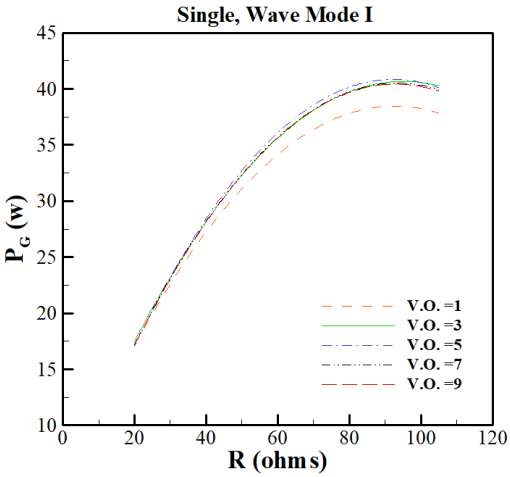

(a) Experimental power in different throttle valve turns

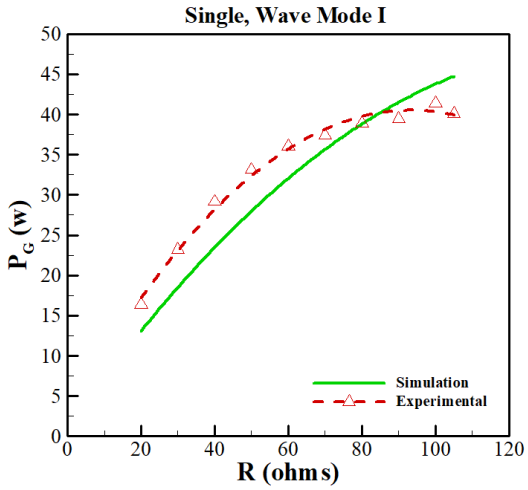

(b) Experimental and numerical power results comparison in resistance range

Figure 19. Captured power in test unit and the simulation

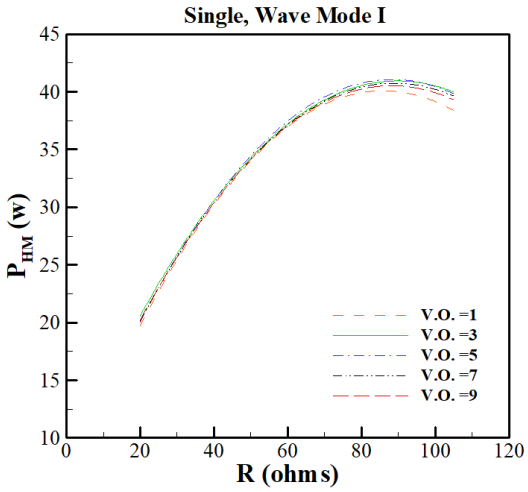

Figure 20. Hydromotor output power in different flow control valve modes

cannot transform to the useful power. Figure 22 illustrates the difference between one opening turn of the flow control valve with the other modes. As can be seen, there is no tangible variation in the generator power of around 40 W in all opening turns except one case. For a better analysis of the result, a closer look at the control valve should be considered. Figure 23 depicts the flow control valve diagram.

The data presented in Figure 23 can confirm why the opening mode of the flow control valve does not affect in some cases. The maximum value of the flow rate passed through hydromotor is 1.9 l/min in this experiment. According to this Figure, for flow rates of less than 20 l/min, the variation of the pressure drop is not distinguishable in different opening modes of the flow

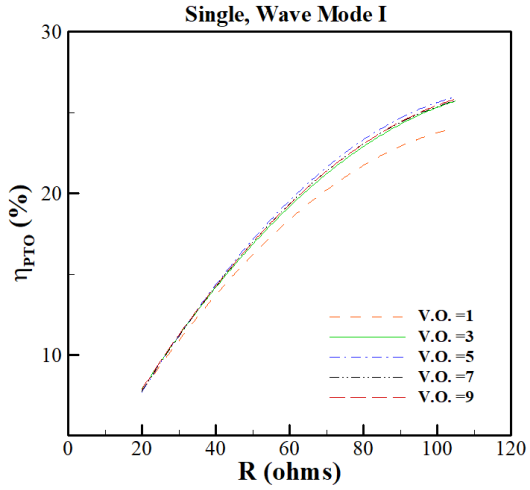

(a) PTO system efficiency in different valve opening modes

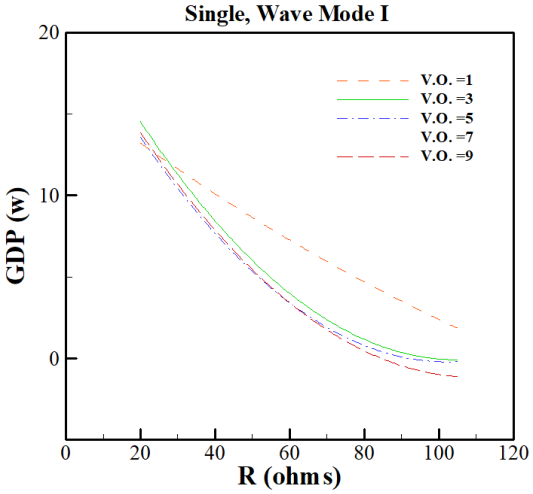

(b) Dissipation among generator and hydromotor in different valve opening modes

Figure 1. efficiency and dissipation of the PTO system

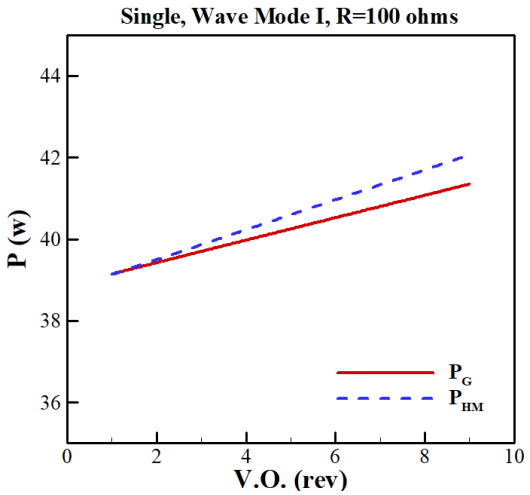

Figure 22. Output power changes with respect to valve opening turns in a 100-ohm resistance

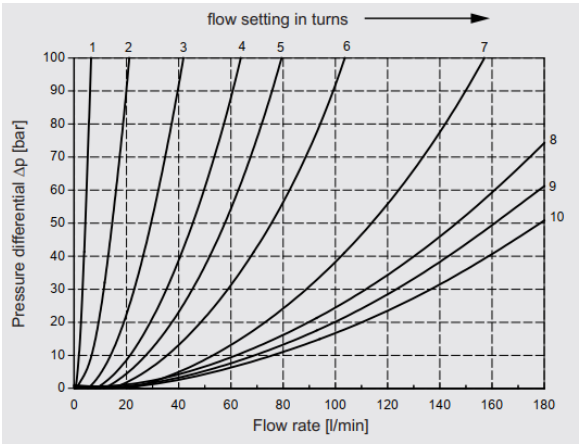

Figure 23. throttle valve performance diagram [24]

control valve, and it is the same for all values of opening turns. However, for the conditions prevailing in the experiment, two initial turns of the valve have a larger pressure drop, but for other numbers of turns, the pressure drop is not significant. Hence, it can be inferred that the total amount of losses is relatively great for the single-turn mode. It should be noted that the pressure drop is 1.5 bar in the oil path from the hydraulic cylinder to the hydromotor for 9 turns of the flow control valve opening. Therefore, the pressure drop is insignificant in the hydraulic circuit path, and a great percentage of pressure loss is attributed to the hydromotor.

In the experiments conducted, the data collection started by turning on the wave-maker and continued until its shutdown. Figure 24 indicates the outputs related to power, efficiency, and pressure difference for 9 turns of the flow control valve and 100-ohm resistive load. As can be seen, all mentioned graphs are stabilized in the approximate duration of 100 seconds. In 100-226 seconds, the outputs are almost constant, and the fluctuations are very negligible. The power changes in the range of 36 to 42 W, and pressure fluctuation is also around 1 bar.

Figure 25 shows the output power of the WEC for different wave heights (20, 25, and 31 cm). The experiment was carried out for 9 turns of the flow control valve. Obviously, with increasing the wave height, the output power will experience a significant increase. For example, the maximum power generated by a 20 cm wave is 3.9 W, and the output is interrupted by increasing the resistance to more than 30 ohms, while this occurs for 25 cm wave in resistance values higher than 90 ohms.

The efficiency curve for the studied heights is presented in Figure 26. The increasing trend of efficiency with wave height is not similar to the power variations. The efficiency at 25 cm wave height is higher than the other wave heights; this is indicated by both the hydromotor and generator performance curves.

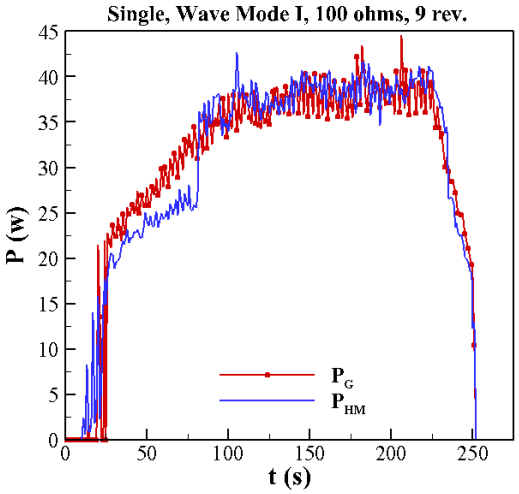

(a) Hydromotor and generator output power

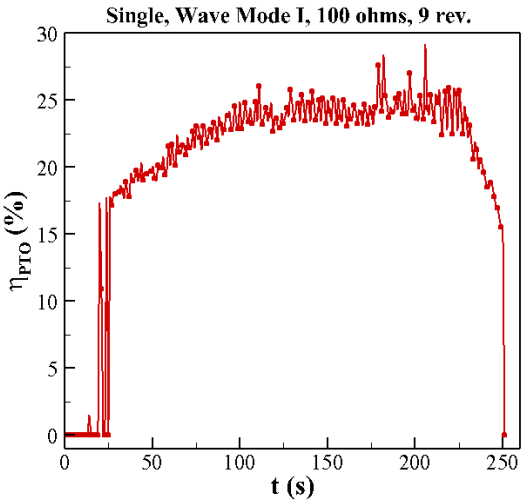

(b) PTO system efficiency

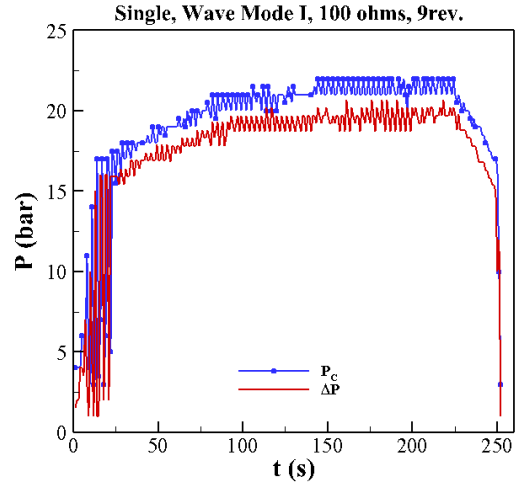

(c) Hydromotor pressure difference and cylinder pressure

Figure 2. Diagrams related to the continuous working of the system in 9th turn valve opening and a 100-ohm resistance

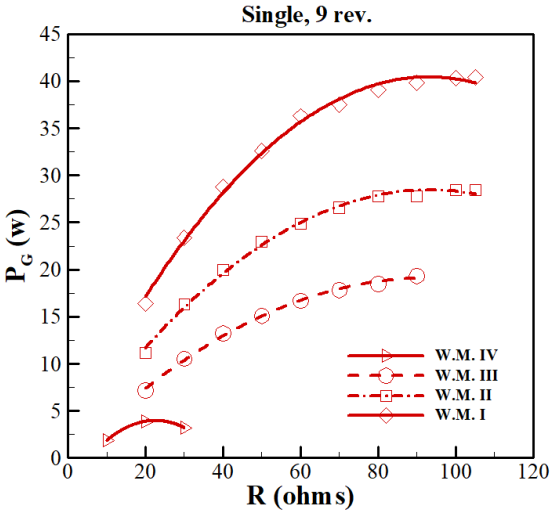

Figure 3. Generator output power for various wave heights in resistance load range by 9 turn applied to the throttle valve

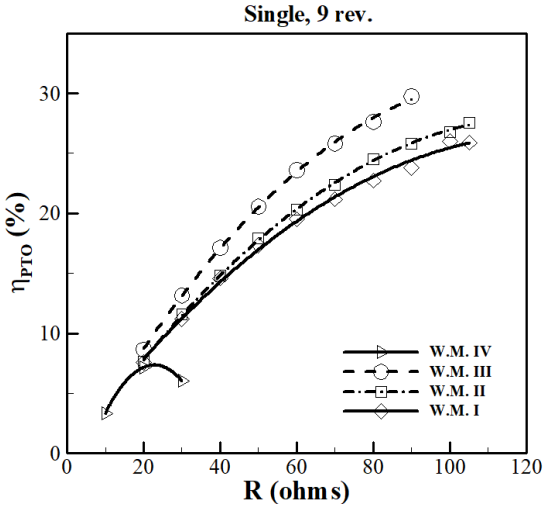

Figure 4. PTO efficiency for various wave heights in resistance load range by 9 turn applied to the throttle valve

Concerning the hydromotor and generator performance curves (Figures 15 and 27), the range of the generator rotational speed is more limited than that of the hydromotor. The rotational speed of the generator and the hydromotor shafts is presented for 4 wave height in the variation range of rheostat resistance as shown in Figure 28. As can be seen, the rotational speed of the generator for a wave with 25 cm height is located at the rated speed limit of the generator, which operates at maximum output power condition.

For the greater height waves, this rotational speed exceeds the nominal speed of the generator, which can explain the difference in the presented efficiency

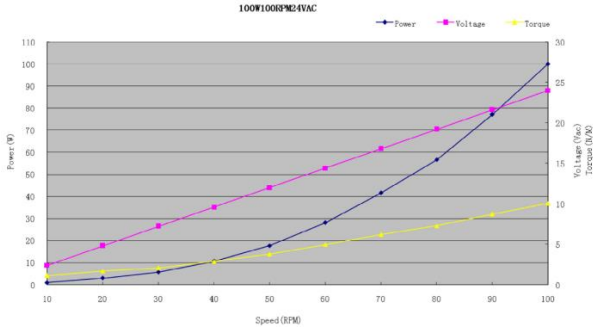

Figure 5. Generator performance diagram [25]

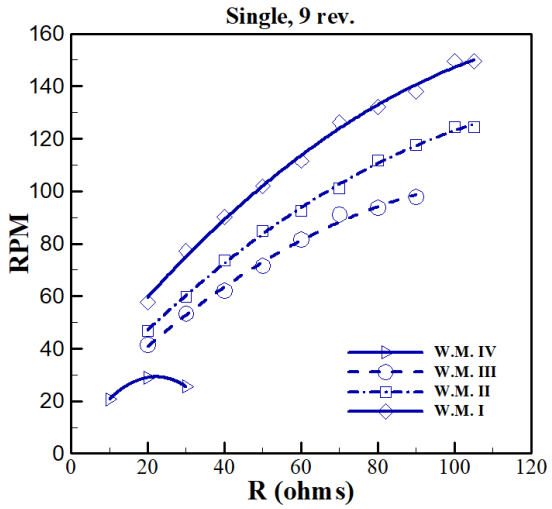

Figure 6. Common shaft rotational velocity for various wave heights in resistance load range by 9 turn applied to the throttle valve

diagrams. The efficiency with a 25 cm wave height and maximum power is equal to 29.7%. Regarding higher power generation with the greater height waves, the generator can be selected according to its rotational speed. Hence, the rated rotational speed of the generator should be placed in the range of rotational speeds determined by the maximum energy and maximum probable waves to achieve the maximum efficiency.

3. 2. Configurations Evaluations The results have been presented for experiments considering a single buoy with a hydraulic cylinder thus far. It should be noted that, as one of the critical results, the maximum output power is recorded for a 100-ohm resistor in the single-buoy single-cylinder case, and achieving the maximum efficiency is subjected to overlap between the rotational speed range of the hydromotor and the generator nominal speed. Since more than a buoy is deployed at the same time in the centipede wave energy converters, the performance of the PTO system is also evaluated by allowing for two buoys to get a better understanding of different configurations of the hydraulic PTO system. Consequently, there are three cases, involving a buoy and a hydraulic cylinder, two buoys connected in series and two buoys connected in parallel that are separately investigated.

The procedure for conducting the tests for series and parallel configurations is similar to the single-buoy test procedure. Figure 29 depicts the power generated in three different configurations of the hydraulic circuit against the resistance variation. Given that the highest power is different between the three configurations of the hydraulic circuit, the diagrams are presented for the single-cylinder and parallel configuration in 9-turn opening mode and for the series configuration in 7-turn opening mode. To this end, the maximum output power is computed as 41.4 W for the single-cylinder state with a 100-ohm resistor, while this value is 41.8 W and 46.43 W in the series and parallel state with an 80-ohm and a 170-ohm, respectivrly. Therefore, in the series and single-cylinder cases, especially in high resistances, the values are very close together and an increase of about 2.25% is observed, but in the parallel case, the two cylinders' synergy is considerable, so a 12.23% increase is achieved relative to the single-cylinder case.

Figure 30 illustrates a comparison of the efficiency in 3 cases. As can be seen, the efficiency in the single-cylinder case is more than that of the parallel and series configurations. Hence, concerning the power and efficiency results, it can be stated that the parallel configuration can be applied to generate the higher power and the single-cylinder counterpart to achieve higher efficiency. The very important achievement obtained from these comparisons is to employ two individual systems in the parallel mode.

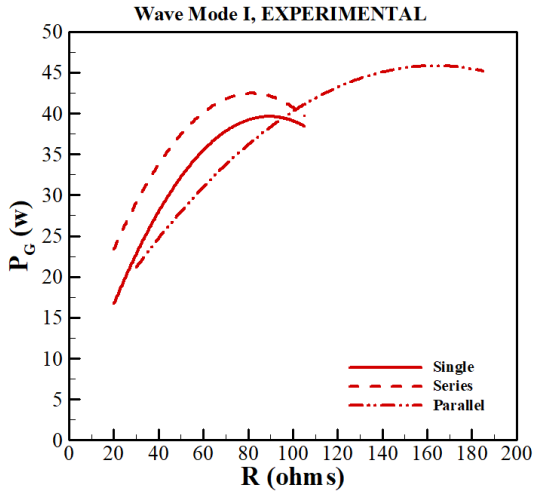

Figure 7. Output PTO system power for single-cylinder and the double type in series and parallel configurations in the range of resistance load (9 turns applied to single and parallel, and 7 turns for series configurations)

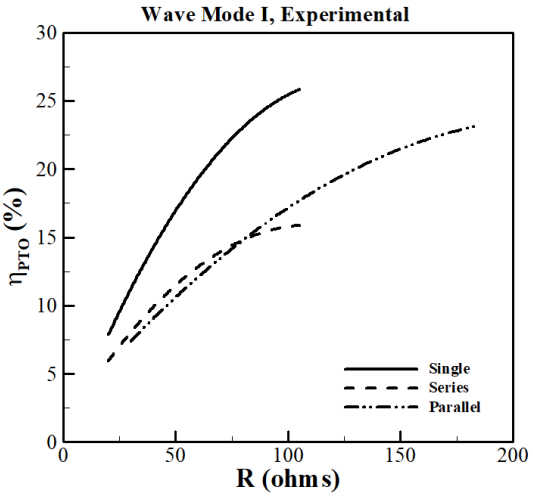

Figure 8. PTO efficiency for single-cylinder and the double type in series and parallel configurations in the range of resistance load (9 turns applied to single and parallel, and 7 turns for series configurations)

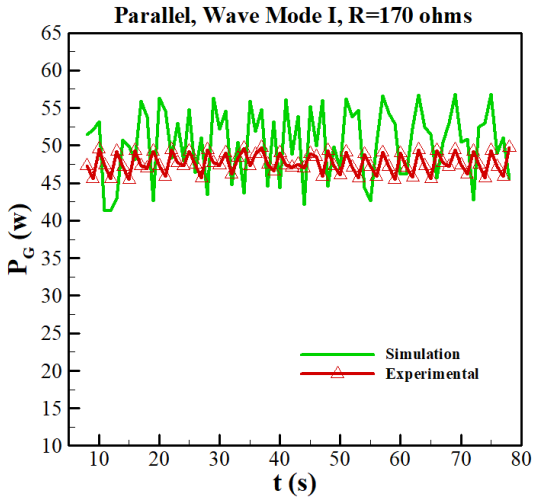

Figure 9. Experimental and numerical contrast for power production in parallel type configuration by applying a 170-ohm resistance

According to the obtained results, both maximum efficiency and generated power can be obtained if two systems are considered completely separate. The point is that for the case where large number of buoys are applied, this strategy results in an increased cost and is not economical. Therefore, the parallel configuration is used in the following to evaluate the increased number of the buoys. In this context, simulations were carried out using Simcenter Amesim software for two, three, and ten buoys. In the curve of efficiency against resistance, the highest efficiency was achieved at the highest resistance at all three configurations. However, the result is that the higher power does not mean higher efficiency. Experimental and simulation results are presented in parallel mode for the 170-ohm resistor in Figure 31. The difference between experimental and simulation results is about 9%.

Due to the appropriate conformance of the numerical and experimental data, the simulation is applied to change the circuit arrangement and to find the optimal number of the hydraulic cylinders in the series and parallel circuits. On the other hand, for the series and parallel cylinders, the results show that, the maximum power is increased by 2.25 and 12.23%, respectively, so the parallel configuration is applied to the numerical simulation considering a wave height of 40 cm and a wave period of 3s. Figure 32 depicts the simulation results for parallel configuration with 2, 3, and 10 cylinders. As can be seen, the resistive load variation is continued to maximize the power generated by the converter. It is worth mentioning that the maximum power for 2, 3, and 10 cylinders are obtained in resistance values of 180, 320, and 1200 ohms, respectively. The interesting point is that by increasing the number of

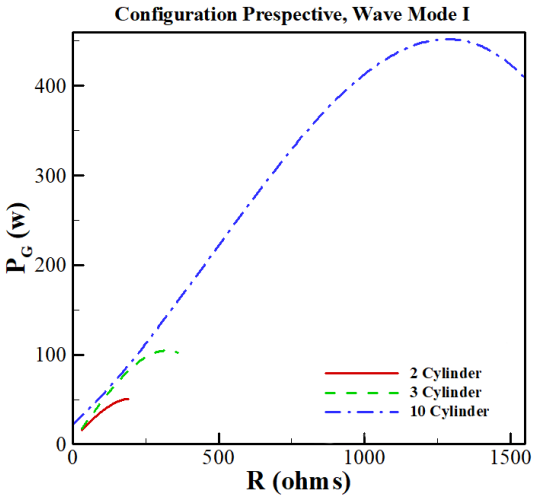

Figure 10. Multi-cylinder influence under the condition of W.M. I

cylinders from 2 to 3, the efficiency of the PTO system decreases from 17.22 to 16.13% while increasing the number of cylinders to 10 leads to a 25.9% increase in the efficiency.

4. CONCLUSION

In this study, the centipede WEC was investigated experimentally and numerically. Experimental tests were performed in the wave tank, and numerical simulations were carried out using Simcenter Amesim software. As the results suited the experiments in terms of compatibility, Simcenter Amesim can be used in more future simulations for hydraulic PTOs. The main

objective of this research was to evaluate the output power and the performance of the PTO system for various configurations of the centipede wave converter. To this end, the maximum output power and efficiency of the PTO system were calculated by defining the resistive load. The effect of the flow rate passing through the flow control valve on the system performance was investigated to achieve maximum power and desired operating conditions of the PTO system. According to the type of Centipede WEC, using separate PTO systems for each arm is not efficient economically. So choosing a proper configuration is of high importance. In the experimental study, three connection configurations were considered for installing hydraulic cylinders together in the hydraulic PTO, including single-buoy (a closed hydraulic loop running by a single buoy, driving the PTO), double-buoy with the series arrangement, and double-buoy with the parallel arrangement (a closed hydraulic loop running by two buoys, driving the same PTO.). First, numerical results were validated by comparing them with experimental results, and then, the best configuration selected. At last numerical simulations were performed for 3- and 10-buoy modes of the selected configuration. Some of the important concluded remarks are stated below:

- The experimental results showed that by increasing the resistive load, the output power increases to a maximum value and then slowly decreases.
- In the experimental tests, the maximum output power of 41.37, 41.8, and 46.43W was obtained considering three different configurations of single-buoy, double-buoy connected in series, and double-buoy connected in parallel, respectively.
- The pressure losses in the hydraulic circuit from cylinder to hydromotor are about 1.5 bar, achieving its maximum value in the hydromotor, but the results showed that the hydromotor output power with optimal resistances is almost completely converted to the output power in the generator.
- In low flow rates, the output power of the generator is not changed significantly by varying the opening mode of the flow control valve, so the increase in the power output from the lowest to the highest opening mode is 7.8%; this parameter can be very effective at high flow rates.
- The PTO system efficiency is 26, 16, and 23% in three different configurations of single-buoy, double-buoy connected in series, and double-buoy connected in parallel, respectively. The efficiency for the single-buoy mode is maximum, but the output power is greater in the parallel configuration than the others. The maximum power and efficiency do not occur at the same time. The parallel configuration is suited to achieve the highest output power, and the single-buoy for maximum efficiency.
- Concerning the selection of the parallel configuration as the desired case, the results obtained from the numerical study showed that the output power significantly increases by increasing the number of buoys followed by the number of hydraulic cylinders in the parallel configuration. Hence, in the configuration of 10 parallel cylinders, with a significant increase in output power, efficiency has also an acceptable increase.

5. AKNOWLEDGEMENTS

The results presented in this article are the outcome of a research project approved by the Supreme Council for Science, Research and Technology (SCSRT). We would like to express our gratitude for the spiritual and funding support of the Mazandaran Provincial Government, the Deputy Governor for Economic Affairs and Resource Development.

6. REFERENCES

1. Tafazzoli, S., Shafaghat, R. and Alamian, R., "Numerical investigation on the multi-body hydrodynamic interactions under Caspian Sea environmental conditions", ***Ocean Engineering***, Vol. 232, (2021), 109048, DOI: 10.1016/j.oceaneng.2021.109048.
2. Tri, N. M., Binh, P. C. and Ahn, K. K., "Power take-off system based on continuously variable transmission configuration for wave energy converter", ***International Journal of Precision Engineering and Manufacturing-Green Technology***, Vol. 5, (2018), 89-101, DOI: 10.1007/s40684-018-0010-0.
3. Yazdi, H., Shafaghat, R. and Alamian, R., "Experimental Assessment of a Fixed On-Shore Oscillating Water Column Device: Case Study on Oman Sea", ***International Journal of Engineering, Transactions C: Aspects***, Vol. 33, (2020), 494-504, DOI: 10.5829/ije.2020.33.03c.14.
4. Henderson, R., "Design, simulation, and testing of a novel hydraulic power take-off system for the Pelamis wave energy converter", ***Renewable Energy***, Vol. 31, (2006), 271-283, DOI: 10.1016/j.renene.2005.08.021.
5. Waters, R., Stålberg, M., Danielsson, O., Svensson, O., Gustafsson, S., Strömstedt, E., Eriksson, M., Sundberg, J. and Leijon, M., "Experimental results from sea trials of an offshore wave energy system", ***Applied Physics Letters***, Vol. 90, (2007), 034105, DOI: 10.1063/1.2432168.
6. Hansen, R. H., *Design and control of the powertake-off system for a wave energy converter with multiple absorbers*. Videnbasen for Aalborg UniversitetVBN, Aalborg Universitet, The Faculty of Engineering and Science. 2013: Department of Energy Technology, Aalborg University. 266.
7. López, I., Andreu, J., Ceballos, S., De Alegría, I. M. and Kortabarria, I., "Review of wave energy technologies and the necessary power-equipment", ***Renewable and Sustainable Energy Reviews***, Vol. 27, (2013), 413-434, DOI: 10.1016/j.rser.2013.07.009.
8. Sarlak, H., Seif, M. S. and Abbaspour, M., "Experimental investigation of offshore wave buoy performance", ***Journal of Marine Engineering***, Vol. 6, (2010).

9. Alamian, R., Shafaghat, R. and Safaei, M. R., "Multi-objective optimization of a pitch point absorber wave energy converter", ***Water***, Vol. 11, (2019), 969, DOI: 10.3390/w11050969.
10. Babarit, A., Guglielmi, M. and Clément, A. H., "Declutching control of a wave energy converter", ***Ocean Engineering***, Vol. 36, (2009), 1015-1024, DOI: 10.1016/j.oceaneng.2009.05.006.
11. Hansen, R. H., Andersen, T. O. and Perdersen, H. C., *Analysis of discrete pressure level systems for wave energy converters*, in *Proceedings of 2011 International Conference on Fluid Power and Mechatronics*. 2011, IEEE. 552-558.
12. Cargo, C. J., Plummer, A. R., Hillis, A. J. and Schlotter, M., "Determination of optimal parameters for a hydraulic power take-off unit of a wave energy converter in regular waves", ***Proceedings of the Institution of Mechanical Engineers, Part A: Journal of Power and Energy***, Vol. 226, (2012), 98-111, DOI: 10.1177/0957650911407818.
13. Bayani, R., Farhadi, M., Shafaghat, R. and Alamian, R., "Experimental Evaluation of IRWEC1, a Novel Offshore Wave Energy Converter", ***International Journal of Engineering, Transactions C: Aspects***, Vol. 29, (2016), 1292-1299. doi: 10.5829/idosi.ije.2016.29.09c.15
14. Hassan, F. A., Mahmoud, M. and Almohammed, O. A., "Analysis of the Generated Output Energy by Different Types of Wind Turbines", ***Journal of Human, Earth, and Future***, Vol. 1, (2020), 181-187.
15. Coiro, D. P., Troise, G., Calise, G. and Bizzarrini, N., "Wave energy conversion through a point pivoted absorber: Numerical and experimental tests on a scaled model", ***Renewable Energy***, Vol. 87, (2016), 317-325, DOI: 10.1016/j.renene.2015.10.003.
16. Alamian, R., Shafaghat, R. and Ghasemi, M., "Experimental evaluation of attenuator WEC in a laboratory wave tank", ***Journal of Marine Engineering***, Vol. 14, (2019), 1-9, DOI: 20.1001.1.17357608.1397.14.28.8.7.
17. Liu, C., Yang, Q. and Bao, G., "Influence of hydraulic power take-off unit parameters on power capture ability of a two-raft-type wave energy converter", ***Ocean Engineering***, Vol. 150, (2018), 69-80, DOI: 10.1016/j.oceaneng.2017.12.063.
18. Kim, S.-J., Koo, W. and Shin, M.-J. *Numerical study on multi-buoy-type wave energy converter platform with hydraulic PTO system*. in ***Oceans*** *2017-Aberdeen*. 2017. IEEE.DOI: 10.1109/OCEANSE.2017.8084920.
19. Tian, H., Zhou, Z. and Sui, Y., "Modeling and Validation of an Electrohydraulic Power Take-Off System for a Portable Wave Energy Convertor with Compressed Energy Storage", ***Energies***, Vol. 12, (2019), 3378, DOI: 10.3390/en12173378.
20. Aghanezhad, M., Shafaghat, R. and Alamian, R., "Experimental Performance Evaluation of a Hydraulic PTO System for Centipede Wave Energy Converter", ***International Journal of Coastal and Offshore Engineering***, Vol. 3, (2020), 35-46, DOI: 10.29252/ijcoe.3.4.35.
21. Alamian, R., Shafaghat, R., Shadloo, M. S., Bayani, R. and Amouei, A. H., "An empirical evaluation of the sea depth effects for various wave characteristics on the performance of a point absorber wave energy converter", ***Ocean Engineering***, Vol. 137, (2017), 13-21, DOI: 10.1016/j.oceaneng.2017.03.036.
22. HYDRAULIC MOTORS MM. https://www.dynahydraulics.com/wp-content/uploads/2017/03/1-MM-1.pdf
23. Hydraulic Motors, Variable Displacement, in HY30-8223/UK, P. Hannifin, Editor. 2014: sweden.
24. Needle Valves with and without Reverse Flow Check Direct-Acting, HYDAC, Editor. p. 1-4.
25. TGET-260-I-100W-100R (AFPMG Three Phase inner rotor). Available from: http://www.china-topgrand.com/product_new/?tid=74&type=85.

Persian Abstract

چکیده

با توجه به شرایط امواج دریای مازندران، به‌کارگیری مبدل‌های انرژی امواج هزارپایی در این دریا، می‌تواند از عملکرد قابل قبولی برخوردار باشد. در این مقاله ضمن معرفی یک مبدل نیمه‌صنعتی تحت عنوان IRWEC2 جهت نصب در دریا، عملکرد سامانه‌ی انتقال توان هیدرولیکی توسعه‌یافته برای این مبدل، به صورت تجربی مورد ارزیابی قرار می‌گیرد. آزمون‌های تجربی در استخر موج دانشگاه صنعتی نوشیروانی بابل انجام شده‌اند. برای طراحی سامانه‌ی انتقال توان هیدرولیکی و ارزیابی اولیه‌ی عملکرد سامانه‌ی PTO، از نرم‌افزار امسیم استفاده شده است. با توجه به استفاده از دو بویه‌ی مجزا، برای استخراج عملکرد بهینه‌ی سامانه‌ی انتقال توان از پیکربندی‌های مختلف سری و موازی برای به‌کارگیری سیلندرهای هیدرولیک مجزا برای هر بویه استفاده شده است. مشخصات موج ورودی، بار مقاوم و نیز میزان گشودگی شیر کنترل جریان، به‌عنوان مهم‌ترین پارامترهای تأثیرگذار بر روی عملکرد مبدل تعریف شده‌اند که مقدار ماکزیمم خروجی ژنراتور در مقادیر معینی از پارامترهای نام‌برده به‌دست می‌آیند. در ابتدا برای اعتبارسنجی فرایندهای تعریف‌شده، نتایج به‌دست آمده از شبیه‌سازی با نرم‌افزار امسیم به نتایج تجربی مقایسه شده است که نتایج شبیه‌سازی‌ها هم‌خوانی بسیار خوبی با نتایج تجربی داشته‌اند. با توجه به نتایج به‌دست آمده، بیشینه توان سامانه‌ی انتقال توان معادل ٤٦ وات به پیکربندی موازی مربوط می‌شود؛ بازدهی سیستم انتقال توان در این حالت ۲۳٪ بوده، خروجی ژنراتور نسبت به حالتی که تنها از یک بویه استفاده شده است، حدود ۱۲٪ افزایش یافته است.